Ductile Ti-Based Bulk Metallic Glasses with High Specific Strength

J.M. PARK, G. WANG, S. PAULY, N. MATTERN, D.H. KIM, and J. ECKERT

Ti-based bulk metallic glasses (BMGs) with large compressive plasticity were developed in the Ti-rich part of Vitreloy series BMGs ($Ti_{65-x}Zr_xCu_9Ni_8Be_{18}$ alloys with $x = 0$, 5, 10, 15, and 20). The current materials exhibit high fracture strength reaching ~2.3 GPa and plastic strains up to ~8.3 pct after partial substitution of Zr by Ti. The plasticity of the investigated alloys strongly depends on the Zr content, which affects the elastic constants, such as Poisson's ratio and shear modulus. This, in turn, has an impact on the shear transformation zone (STZ) volume and, hence, on the shear banding of the glasses.

DOI: 10.1007/s11661-010-0416-y

I. INTRODUCTION

BULK metallic glasses (BMGs) are generally recognized as advanced engineering materials because of their superior physical, chemical, and mechanical properties compared to their crystalline counterparts.[1–3] Among these BMGs, Zr-(Ti, Nb)-Cu-Ni-(Al, Be) alloys (Vitreloy series) are well known due to their high glass-forming ability (GFA), excellent corrosion resistance, large plastic deformability in the supercooled liquid region, and good mechanical properties, which are manifested by a high yield strength and a large elastic strain limit.[4–8] However, these Zr-based alloys contain late transition metals (LTMs) (*e.g.*, Ni and Cu) with a high mass density and, hence, are not attractive for applications where light weight is required. Seen from this angle, Ti-based alloys have a larger potential owing to their lower density and relatively low cost.[9,10] Therefore, extensive research has been conducted in the Ti-rich corner of the (Zr,Ti)-(Cu,Ni)-Be pseudo-ternary glass-forming system,[11,12] and only recently, low density Ti-Zr-Be–based BMGs with improved specific strength excluding LTMs (*e.g.*, Fe, Ni, Cu, and Sn) have been developed.[13,14] These results imply that the adjustment of the LTM content in alloys of the Vitreloy series allows tailoring of the yield strength while still maintaining a large specific strength.[15]

On the other hand, plasticity is also a desirable property for BMGs for widespread practical application. Since the plastic deformation of BMGs is highly inhomogeneous at room temperature through the formation of shear bands, they exhibit limited plastic strain (<1 pct) and are prone to catastrophic failure.[1,2] The macroscopic room temperature plasticity of BMGs is strongly related to their solidification history, sample size, and intrinsic elastic properties.[16–21] Recently, intrinsically ductile BMGs have been developed for some special alloy systems.[22–25] For example, Schroers *et al.* reported on a monolithic Pt-based BMG with a global plasticity of 20 pct.[22] It has been argued that controlling the elastic constants can effectively improve plasticity and fracture toughness,[21,22] whereupon intrinsically ductile BMGs tend to have a higher Poisson's ratio (ν) or lower shear-to-bulk modulus ratio, G/K. The threshold value of ν has been found to be 0.31 to 0.32, and the G/K ratios of ductile BMGs were identified to be smaller than 0.41 to 0.43, respectively.[22,26]

For the Ti-based BMG $Ti_{40}Zr_{25}Cu_{12}Ni_3Be_{20}$ subjected to different cooling rates, the critical ν value or G/K ratio is somewhat higher than the values obtained for other BMGs ($\nu > 0.35$ or $G/K < 0.33$).[27–29] When BMGs have a high ν value or a low G/K ratio, shear bands are easily initiated and multiplied during deformation and the plastic strain therefore increases. This reveals that the tendency of the shear stress to concentrate in shear bands rather than in cracks plays a crucial role in the enhancement of the deformation behavior.[20,42]

In this study, we selected the Ti-rich $Ti_{65}Cu_9Ni_8Be_{18}$ glassy alloy in the (Zr,Ti)-(Cu,Ni)-Be pseudo-ternary glass-forming system as a starting composition having a high specific strength.[17] By changing the composition of these alloys, our focus is on the influence of the Zr content on the mechanical properties, especially on plasticity. We will discuss the mechanism underlying plastic flow in the framework of self-organized criticality behavior, which will be associated with the elastic parameters, such as Poisson's ratio, shear modulus, and bulk modulus.

J.M. PARK and G. WANG, Guest Scientists, S. PAULY, Research Staff Member, N. MATTERN, Head of Department, and J. ECKERT, Director and Professor, are with the Institute for Complex Materials, IFW Dresden, D-01171 Dresden, Germany. Contact e-mail: j.m.park@ifw-dresden.de D.H. KIM, Professor, is with the Center for Non-Crystalline Materials, Department of Metallurgical Engineering, Yonsei University, Seoul 120-749, Republic of Korea and the Institute of Materials Science, TU Dresden, D-01062 Dresden, Germany.

Manuscript submitted March 25, 2010.
Article published online September 22, 2010

II. EXPERIMENTAL PROCEDURE

A series of $Ti_{65-x}Zr_xCu_9Ni_8Be_{18}$ BMGs with $x = 0$, 5, 10, 15, and 20 (labeled as Z0: $Ti_{65}Cu_9Ni_8Be_{18}$, Z5: $Ti_{60}Zr_5Cu_9Ni_8Be_{18}$, Z10: $Ti_{55}Zr_{10}Cu_9Ni_8Be_{18}$, Z15: $Ti_{50}Zr_{15}Cu_9Ni_8Be_{18}$, and Z20: $Ti_{45}Zr_{20}Cu_9Ni_8Be_{18}$) was prepared by arc melting the pure elements in an argon atmosphere followed by copper mold casting into cylindrical rods with a diameter of 2 mm and a length of 50 mm. X-ray diffraction (XRD; Rigaku CN2301, Tokyo, Japan) and high-resolution transmission electron microscopy (HRTEM; JEM 2010F, Tokyo, Japan) were performed to characterize the structure. Thin foils for TEM were prepared by conventional ion milling (PIPS; Gatan model 691, Vienna, OH). In order to evaluate the mechanical properties under compression, cylindrical specimens with an aspect ratio of 2:1 were prepared and tested under quasi-static loading using an initial strain rate of 1×10^{-4} s^{-1} at room temperature. In order to assure the reliability of the mechanical property data, the values of the compressive mechanical properties were determined from the average values of minimum four measurements for each sample. The lateral and fracture surface morphologies of the deformed samples were investigated by scanning electron microscopy (SEM; Hitachi S-2700, Tokyo, Japan). The elastic properties were determined by ultrasound velocity measurements (Olympus Panametrics-NDT 5900PR, MA) under 20 MHz shear wave and 100 MHz longitudinal wave.

III. RESULTS AND DISCUSSION

Figure 1 shows the room temperature engineering stress-strain curves of the as-cast alloys Z0, Z5, Z10, Z15, and Z20, respectively. The stress-strain curves of all investigated glassy alloys exhibit a serrated flow behavior after yielding. The compressive mechanical properties and the density, ρ, are summarized for all investigated alloys in Table I. For comparison, the parameters of other Ti-based BMGs and Vitreloy series alloys are also listed in Table I. The current materials exhibit high fracture strengths reaching 2.3 GPa (Z0) and large plastic strains up to 8.3 pct (Z10). With increasing the Zr content from 0 to 20 at. pct, both the yield and the fracture strength continuously decrease from 2183 to 1980 MPa and from 2250 to 2008 MPa, respectively. Meanwhile, the compressive plastic strain shows a maximum value at $x = 10$, and then slightly decreases. Their specific strength is expressed as the yield strength divided by the density of the alloy. Normally, the Ti content in most Ti-based BMGs is lower than 50 at. pct,[9–11,13] and high Zr, low Cu, and Ni bearing BMGs tend to be lighter than previously reported Zr- and Ti-based BMGs.[4,6–8] A ~20 pct advantage over Vitreloy alloys in specific strength is achieved. According to this point of view, the specific strengths of Z5 and Z10 with high Ti content (55 at. pct ≤ Ti ≤ 60 at. pct) in this work are the largest values reported so far without a significant sacrificing of the GFA (Table I).

Figure 2(a) shows an enlarged part of the stress-strain curve for Z10, as marked by the dashed squared region

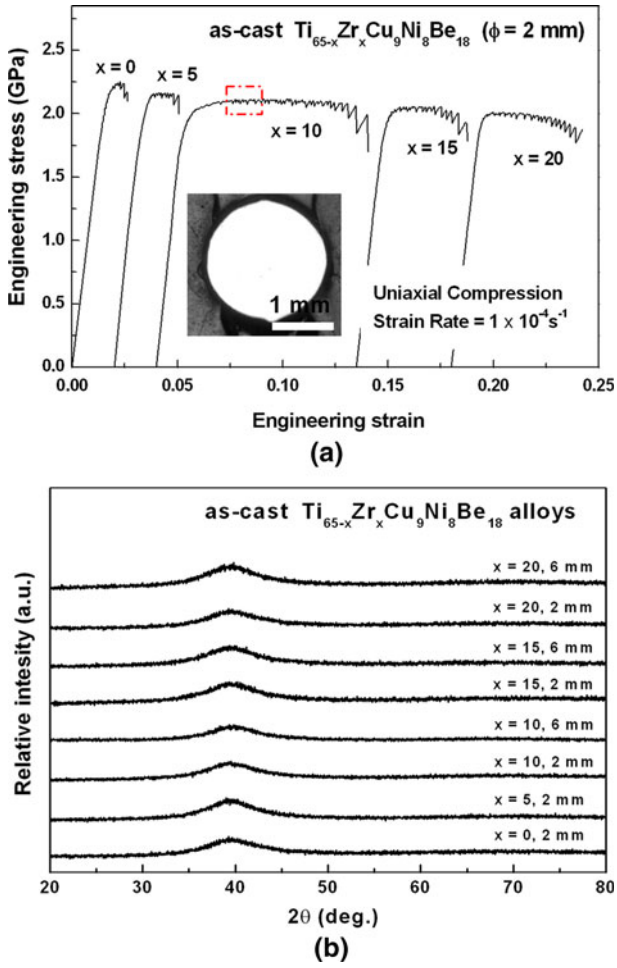

Fig. 1—Room temperature engineering (*a*) stress-strain curves and (*b*) XRD patterns of the as-cast Z0, Z5, Z10, Z15, and Z20 rod samples, respectively. The inset shows the microstructure of the cross section of Z10 (2-mm-diameter rod sample).

in Figure 1. The area of the hatched triangle represents the elastic energy density of a single serration event for this alloy. A sequence of serration events indicates the aggregation and release of deformation energy during plastic deformation, which manifests itself as discrete bursts of plasticity.[30] The so-called shear avalanches of a sudden stress drop can force the sample to self-organize into a critical state.[31] To further characterize the plastic flow behavior of the present alloys, a statistical analysis of the serration events was conducted. One serration event includes the process of elastic energy accumulation and the process of elastic energy release (Figure 2(a)). The elastic energy density of one serration event ($\Delta\delta$) is $\Delta\delta = \frac{1}{2}\Delta\sigma_E\Delta\varepsilon_E$, where $\Delta\delta_E$ and $\Delta\varepsilon_E$ are the elastic stress and elastic strain of one serration event, respectively (Figure 2(a)).[30] $\Delta\delta$ provides a parameter reflecting the dynamics of shear deformation in BMGs, and to further characterize plastic flow, we plot the elastic energy density distribution, which was obtained from all serrations occurring during plastic flow (Figure 2(b)). It has been suggested that the cumulative probability distribution follows a power law,[32] according to the following equation:

Table I. Glass Forming Ability, Physical, and Mechanical Properties for a Variety of Ti-Based BMGs Together with Vitreloy Series Alloys*

Composition	D_{max} (mm)	ρ (kg/m^3)	σ_y (MPa)	σ_{max} (MPa)	ε_y (Pct)	ε_p (Pct)	σ_c (N·m/kg)	Ref.
$Ti_{65}Cu_9Ni_8Be_{18}$ (Z0)	2	4.84	2183	2250	1.9	0.7	4.5×10^5	this work
$Ti_{60}Zr_5Cu_9Ni_8Be_{18}$ (Z5)	4	4.98	2120	2154	1.8	1.4	4.3×10^5	this work
$Ti_{55}Zr_{10}Cu_9Ni_8Be_{18}$ (Z10)	6	5.03	2050	2113	1.8	8.3	4.1×10^5	this work
$Ti_{50}Zr_{15}Cu_9Ni_8Be_{18}$ (Z15)	6	5.19	2014	2060	1.8	3.5	3.9×10^5	this work
$Ti_{45}Zr_{20}Cu_9Ni_8Be_{18}$ (Z20)	6	5.25	1980	2008	1.8	4.4	3.8×10^5	this work
$Zr_{41.2}Ti_{13.8}Cu_{12.5}Ni_{10}Be_{22.5}$ (Vit1)	>20	6.07	1737	1774	2.0	1	3.5×10^5	4
$Zr_{46.75}Ti_{8.25}Cu_{7.5}Ni_{10}Be_{27.5}$ (Vit4)	>20	5.99	1820	1890	2.0	2	3.3×10^5	8
$Zr_{52.5}Ti_5Cu_{17.9}Ni_{14.6}Al_{10}$ (Vit105)	>20	6.55	1850	1900	2.0	2	3.5×10^5	6
$Zr_{57}Cu_{15.4}Ni_{12.6}Al_{10}Nb_5$ (Vit106)	>10	6.68	1785	1800	2.0	0.5	3.7×10^5	7
$Ti_{45}Cu_{25}Ni_{15}Sn_3Be_7Zr_5$	6	6.93	2355	2480	1.8	4	3.4×10^5	9
$Ti_{40}Zr_{10}Cu_{34}Pd_{14}Sn_2$	10	6.85	2000	2050	2.2	3.5	2.9×10^5	10
$Ti_{40}Zr_{25}Cu_{12}Ni_3Be_{20}$	14	5.38	1680	1780	1.8	5	3.1×10^5	11
$Ti_{45}Zr_{20}Be_{35}$	6	4.59	1795	1860	1.9	0.3	3.9×10^5	13
$Ti_{40}Zr_{25}Be_{30}Cr_5$	8	4.89	1720	1900	1.9	3.5	3.6×10^5	13

*Maximum diameter for glass formation D_{max}, density ρ, yield stress σ_y, yield strain ε_y, ultimate compressive stress σ_{max}, plastic strain ε_p, and specific strength σ_c. Average values of ρ, σ_y, ε_y, σ_{max}, and ε_p are listed. The measurement errors in ρ, σ_y, ε_y, σ_{max}, and ε_p are estimated to be in the range ±0.02, ±20 MPa, ±50 MPa, ±0.05 pct, and ±2 pct, respectively.

$P(\geq \Delta\delta) = A\Delta\delta^{-\beta} \exp\left[-(\Delta\delta/\delta_C)^2\right]$, where A is a normalization constant, β is a scaling exponent, and δ_C is the cut-off elastic energy density. We apply this equation also to the present samples, and in doing so, A, β, and δ_C are fitting parameters (Figure 2(b)).[32] It is obvious that the scaling exponent, β, remains constant at 0.40 ± 0.01 with increasing Zr content. However, the cut-off elastic energy density, δ_C, increases from 17,337 J/m^3 (Z0) to 95,585 J/m^3 (Z15) and then slightly decreases to 87,668 J/m^3 (Z20). The universal β value of 0.40 indicates that the serrated flow follows a self-organized critical behavior.[31,32] The change in δ_C is associated with the plastic strain variation with increasing Zr content. An important feature of the self-organized critical behavior is a self-similar or scale-free pattern, which means that characteristic features on a small scale appear to be the same as the ones on larger scales.

The enlarged stress-strain curves for two selected samples, which exhibit a large variation in plastic strain, *viz*. Z5 and Z10, are shown in Figure 2(c). The profile of the stress-strain curve of the BMG with larger plasticity (Z10) indicates that a large serration event is frequently followed by a succession of serration events with smaller amplitude. This behavior is analogous to that of a stress shock due to a rising strain, which is often followed by several aftershocks of smaller magnitude. The smaller stress undulations in the aftershocks, *i.e*., the smaller serration events, can drive the system to self-organize into a new critical state, and as a consequence, this creates more serrations during plastic flow for this alloy. For Z5, the alloy with the smaller plasticity, the serration events are of larger magnitude and are not followed by smaller stress bursts; *i.e*., after the main shock, smaller aftershocks are mainly absent. This, in turn, means that the self-organization behavior of this alloy is weaker (inset of Figure 2(c)). This result is believed to indicate that the increase in the shear band density affects the elastic energy stored in the serration events; *i.e*., the elastic energy is spread more homogeneously over several serration events with smaller amplitude. Thus, a significant self-organized critical behavior is achieved and the plasticity is improved by multiplication of shear bands.

The fractured Z0, Z10, and Z15 samples were examined further by SEM (Figure 3). All samples roughly fracture along the maximum shear plane, which is inclined by about 42 deg to the direction of the applied load, as shown in Figures 3(a), (c), and (e). The lateral surface and the fracture surface morphologies of the samples are slightly different. The Ti-rich BMG (Z0) exhibits only few and scattered shear bands on the lateral surface, obviously reflecting a low plasticity. With increasing plasticity, also the density of shear bands on the whole surface region increases, as can be seen for alloys Z10 and Z15 (Figures 3(c) and (e)). Primary shear bands with an intershear band distance of 100 to 200 μm are generated parallel to the fracture plane, as marked by the arrows in the inset of Figure 3(c). Next to the primary shear bands, some irregularly shaped secondary shear bands with an intershear band distance of 20 to 40 μm form perpendicular to the applied load (inset of Figure 3(c)). These two kinds of shear bands are highly intersecting with each other, thus, considerably enhancing the shear band density and gradually reducing the intershear band distance, which effectively promotes plasticity. The inset of Figure 3(c) shows a pronounced tendency for branching of shear bands during their propagation, thereby retarding the formation of a detrimental shear band. Moreover, large shear steps are observed to accommodate the excessive strain before fracture. In short, the high density of shear bands operating in the Z10 and Z15 samples reveals that the relatively more uniform plastic deformation occurs by multiple shear banding rather than shear localization and increases the macroscopic plasticity.

In addition, the fracture surface morphology of the failed samples was carefully investigated. As depicted in Figure 3(b), alloy Z0 displays a typical vein pattern, which is characteristic of metallic glasses and which

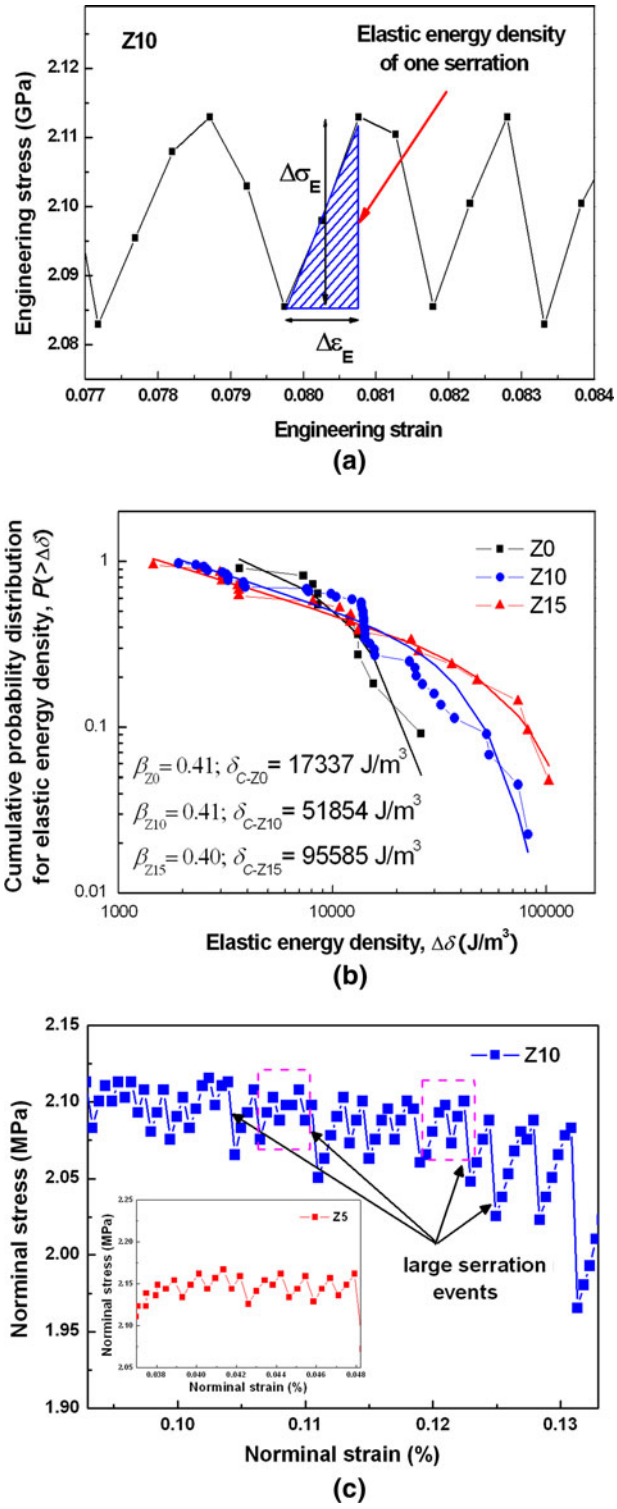

Fig. 2—(*a*) Elastic energy density for one serration event extracted from the data for the alloy Z10 and (*b*) cumulative probability distributions for the elastic energy densities obtained for the as-cast Z0, Z10, and Z15 samples, respectively. The scattering points are experimentally measured from the compressive stress-strain curves. The solid lines are fitted by $P(\geq\Delta\delta) = A\Delta\delta^{-\beta} \exp[-(\Delta\delta/\delta_C)^2]$ and detail plastic stress-strain curves (b) for the as-cast Z5 and Z10 alloys. The serration events with smaller elastic energy densities are covered by red boxes.

originates from local heating.[33] On the other hand, the fractographic analysis of alloys Z10 and Z15 indicates smaller and less developed vein patterns compared to those found for alloy Z0 (Figures 3(d) and (f)). Moreover, Figure 3(d) shows a relatively rough and complex fracture surface morphology containing veinlike features (marked i), a riverlike pattern (marked ii), and smooth regions (marked iii).[34] Such a surface morphology can be explained by presuming that locally the stress is multiaxial and that there is a normal component acting on the fracture plane during shear deformation and fracture.[35]

Normally, enhanced plastic strain to failure has been observed in metallic glass matrix composites containing heterogeneities on different length scales, such as medium-range ordering, nanocrystalline particles, and ductile crystalline phases.[23,36–40] Also, possible variations in the elastic constants, *e.g.*, Poisson's ratio or shear modulus, could explain the observed plastic strain.[21,22,25,26]

In order to check the first hypothesis that the existence of potential microstructural heterogeneities might result in the plasticity observed, high-resolution TEM analysis was performed. Figure 4 shows high-resolution TEM images of selected alloys, namely, Z0 and Z10. For all samples, there is a homogeneous contrast without any crystalline fringes confirming a single-phase amorphous structure. Although both alloys show a quite different deformation behavior, it is believed that both samples have a similar, amorphous structure. In addition, the constant β value (*cf.* Figure 2(b)) suggests that the plastic deformation mechanism of all samples does not change significantly.[41] Since atomic-scale inhomogeneities can be thus excluded as reason for the variation in plastic strain, we will focus on the elastic constants in the following.

It is believed that the intrinsic elastic properties of BMGs can be controlled properly by tuning the interatomic interaction or the packing density.[21,22] In this study, Zr addition may be effective to modulate the atomic bonding and configuration, since Zr has the largest atomic radius (= 0.216 nm) among the constituent elements and zero enthalpy of mixing with the major constituent elements (Zr-Ti: 0 kJ/mol) rather than a large negative enthalpy of mixing (Zr-Ni: –49 kJ/mol, Zr-Cu: –23 kJ/mol, and Zr-Be: –43 kJ/mol).

In general, the elastic behavior is associated with the atomic packing density (ρ_A).[46] Based on the equation $\rho_A = (N_A \cdot \rho)/M_A$ (where N_A is Avogadro's constant, ρ is the density of the alloy, and M_A is the atomic mass), the atomic packing densities of five BMGs are calculated (Table II). It is obvious that the atomic density decreases with increasing Zr content, suggesting a rather loose packing of atoms. Loose packing can result in lower yield strength and higher plastic strain, which is consistent with the compression test results (Table I). However, when the Zr content exceeds 10 at. pct, the influence of the local atomic structure becomes more significant. In this case, icosahedral-like short-range ordered clustering is pronounced,[47] which is not

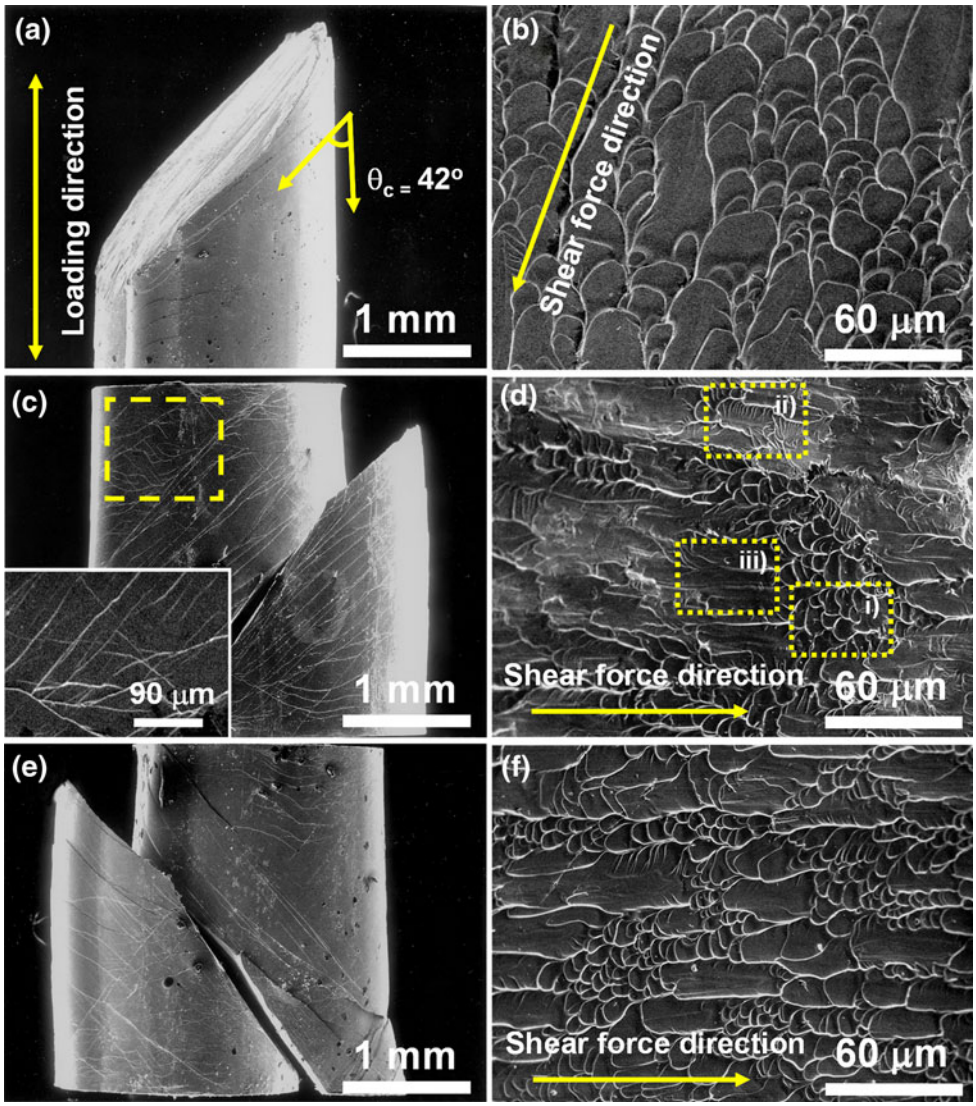

Fig. 3—Secondary electron SEM images taken from the failed Z0, Z10, and Z15 samples, respectively: overall shape of failed samples (*a*) Z0, (*c*) Z10, and (*e*) Z15; and fracture surface morphology (*b*) Z0, (*d*) Z10, and (*f*) Z15, respectively. The insets show highly magnified images for the dashed square regions.

desirable to increase the free volume and to improve the plasticity and, thus, results in a reduction of the plastic strain to failure. Therefore, the maximum plasticity appears for alloy Z10.

The elastic constants obtained from ultrasound velocity measurements are given in Table II. The G/K ratio and the value for ν of all alloys investigated are plotted as a function of the Zr content in Figure 5(a). With increasing Zr content, G/K and ν show a maximum at Zr 10 at. pct, while the bulk modulus continuously decreases (Figure 5(a) and Table II). The plastic strains for same materials are plotted as a function of G or ν in Figure 5(b). With a lower value for G, or equivalently a higher value for ν, the materials undergo more uniform shear deformation and the plasticity is enhanced. Thus, the enhancement of plasticity can be associated with a decrease in G/K or, equivalently, the increase of ν reflecting the decrease of the shear resistance. Hence, the intrinsic toughness of the currently investigated alloys can be effectively controlled *via* tuning of the composition (Zr addition).

The increase in the Poisson's ratio indicates that the effective shear transformation zone (STZ) volume increases.[42] Since the maximum elastic strain required for shear band nucleation in BMGs can initiate a collective motion of STZs,[43] a larger STZ volume enables a smaller number of STZs to be activated for the nucleation of a shear band. Furthermore, a STZ with a larger volume can produce a larger internal stress concentration, and new flow events (STZs) can then be more easily activated by thermal energy.[42] Therefore, a high value for ν, or likewise a large STZ volume, can effectively improve the shear deformation ability of BMGs and leads to the generation of multiple shear bands. These release the local stress concentrations in the material and accommodate the shear strain

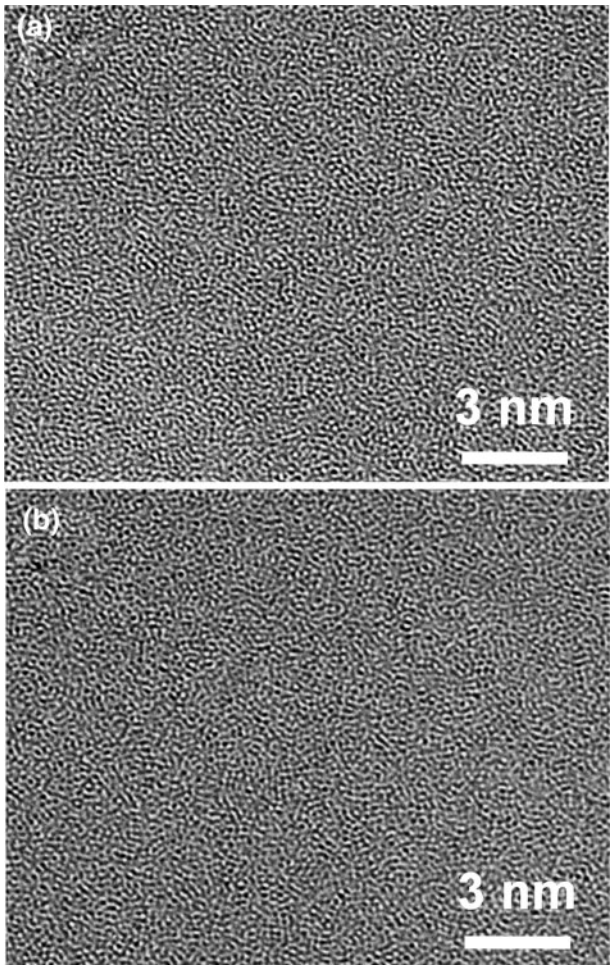

Fig. 4—High-resolution TEM image for the as-cast alloys Z0 and Z10, respectively.

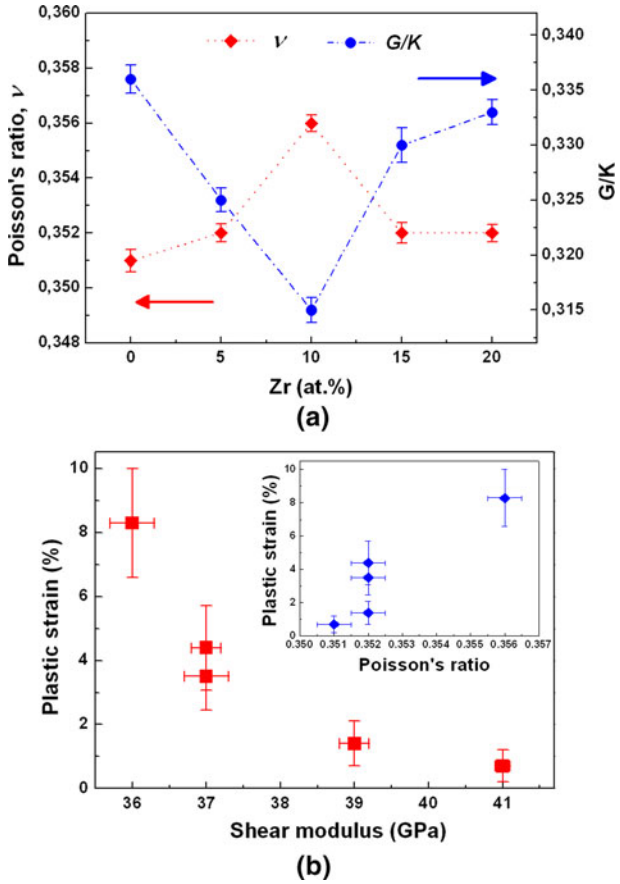

Fig. 5—(*a*) Poisson's ratio ν and G/K ratio as a function of Zr content and (*b*) plastic strain ε_p *vs* shear modulus G and Poisson's ratio ν for the as-cast glassy alloys Z0, Z5, Z10, Z15, and Z20.

Table II. Atomic Density and Elastic Constants for the As-Cast Z0, Z5, Z10, Z15, and Z20 Alloys, Respectively*

Name	Composition (At. Pct)	Atomic Density (Atoms/nm^3)	ν	E (GPa)	G (GPa)	K (GPa)	G/K
Z0	$Ti_{65}Cu_9Ni_8Be_{18}$	67.5	0.351 ± 0.0005	110 ± 0.2	41 ± 0.1	122 ± 0.7	0.336 ± 0.001
Z5	$Ti_{60}Zr_5Cu_9Ni_8Be_{18}$	66.2	0.352 ± 0.0005	106 ± 0.3	39 ± 0.2	120 ± 0.5	0.325 ± 0.0013
Z10	$Ti_{55}Zr_{10}Cu_9Ni_8Be_{18}$	63.8	0.356 ± 0.0005	98 ± 0.5	36 ± 0.3	114 ± 0.5	0.315 ± 0.002
Z15	$Ti_{50}Zr_{15}Cu_9Ni_8Be_{18}$	62.9	0.352 ± 0.0005	100 ± 0.4	37 ± 0.3	112 ± 0.4	0.330 ± 0.0026
Z20	$Ti_{45}Zr_{20}Cu_9Ni_8Be_{18}$	61.0	0.352 ± 0.0005	101 ± 0.4	37 ± 0.2	111 ± 0.4	0.333 ± 0.0016

*Atomic density, Poisson's ratio ν, Young's modulus E, shear modulus G, bulk modulus K, and G/K ratio.

more homogeneously during plastic deformation. The release of elastic energy mainly activates flow events (STZs) in liquidlike solids, and the elastic energy of serrations can be consumed by the STZs through configurational hopping.[44,45] Since the δ_C value is associated with the amount of activated STZs, a large value for δ_C indicates that more STZs are triggered to carry the shear deformation, and macroscopically, this should be detectable as increased plastic strain. Consequently, controlling the elastic constants can provide a useful guideline to manage the resulting mechanical structure in the BMGs investigated in this work.

IV. SUMMARY

The partial substitution of Zr for Ti in Ti-rich $Ti_{65-x}Zr_xCu_9Ni_8Be_{18}$ (x = 0 to 20) BMGs yields high specific strengths and large plastic strains. Especially, the $Ti_{55}Zr_{10}Be_{18}Cu_9Ni_8$ glassy alloy exhibits a high ultimate compressive strength of ~2.1 GPa and a maximum compressive plasticity of ~8.3 pct, along with a strong self-organized intermittent plastic flow. The large compressive plasticity can be correlated with a high Poisson's ratio and a low shear modulus, which can be traced back microscopically to an increase of the STZ volume. These findings suggest that tuning of the elastic

constants by addition of Zr in Ti-Cu-Ni-Be BMG can successfully improve the mechanical properties of Ti-based BMGs, especially with regard to plasticity.

ACKNOWLEDGMENTS

This work was supported by the Global Research Laboratory Program of the Korea Ministry of Education, Science and Technology. Stimulating discussions with J.H. Han, K.B. Kim, and R. Li are gratefully acknowledged. GW acknowledges the fellowship support from the Alexander von Humboldt Foundation. SP furthermore acknowledges the financial support granted by the program "Promotionsförderung des Cusanuswerks."

REFERENCES

1. W.L. Johnson: *MRS Bull*., 1999, vol. 24, pp. 42–62.
2. A. Inoue: *Acta Mater*., 2000, vol. 48, pp. 279–306.
3. M.F. Ashby and A.L. Greer: *Scripta Mater*., 2006, vol. 54, pp. 321–26.
4. A. Peker and W.L. Johnson: *Appl. Phys. Lett*., 1993, vol. 63, pp. 2342–44.
5. C.C. Hay, C.P. Kim, and W.L. Johnson: *Appl. Phys. Lett*., 1999, vol. 75, pp. 1089–91.
6. M.E. Siegrist and J. Löffler: *Scripta Mater*., 2007, vol. 56, pp. 1079–82.
7. H. Choi-Yim, R.D. Conner, F. Szuecs, and W.L. Johnson: *Scripta Mater*., 2001, vol. 45, pp. 1039–45.
8. H.B. Yu, J. Hu, X.X. Xia, B.A. Sun, X.X. Li, W.H. Wang, and H.Y. Bai: *Scripta Mater*., 2009, vol. 61, pp. 640–43.
9. Y.C. Kim, W.T. Kim, and D.H. Kim: *Mater. Sci. Eng. A*, 2004, vols. 375–377, pp. 127–35.
10. S.L. Zhu, X.M. Wang, and A. Inoue: *Intermetallics*, 2008, vol. 16, pp. 1031–35.
11. F.Q. Guo, H.J. Wang, S.J. Poon, and G.J. Shiflet: *Appl. Phys. Lett*., 2005, vol. 86, p. 091907.
12. Y.C. Kim, J.M. Park, J.K. Lee, D.H. Bae, W.T. Kim, and D.H. Kim: *Mater. Sci. Eng. A*, 2004, vols. 375–377, pp. 749–53.
13. G. Duan, A. Wiest, M.L. Lind, A. Kahl, and W.L. Johnson: *Scripta Mater*., 2008, vol. 58, pp. 465–68.
14. Y. Zhang, W.G. Zhang, J.P. Lin, G.J. Hao, G.L. Chen, and P.K. Liaw: *Metall. Mater. Trans. A*, 2010, vol. 41A, pp. 1670–76.
15. J.M. Park, Y.C. Kim, W.T. Kim, and D.H. Kim: *Mater. Trans*., 2004, vol. 45, pp. 595–98.
16. R.D. Conner and W.L. Johnson: *Scripta Mater*., 2006, vol. 55, pp. 645–48.
17. J.M. Park, H.J. Chang, K.H. Han, W.T. Kim, and D.H. Kim: *Scripta Mater*., 2005, vol. 53, pp. 1–6.
18. H. Guo, P.F. Yan, Y.B. Wang, J. Tan, Z.F. Zhang, M.L. Sui, and E. Ma: *Nature Mater*., 2007, vol. 6, pp. 735–39.
19. Y.J. Huang, J. Shen, and J.F. Sun: *Appl. Phys. Lett*., 2007, vol. 90, p. 081919.
20. J.M. Park, G. Wang, R. Li, N. Mattern, J. Eckert, and D.H. Kim: *Appl. Phys. Lett*., 2010, vol. 96, p. 031905.
21. X.J. Gu, S.J. Poon, G.J. Shiflet, and M. Widom: *Acta Mater*., 2008, vol. 56, pp. 88–94.
22. J. Schroers and W.L. Johnson: *Phys. Rev. Lett*., 2004, vol. 93, p. 255506.
23. J. Das, M.B. Tang, K.B. Kim, R. Theissmann, F. Baier, W.H. Wang, and J. Eckert: *Phys. Rev. Lett*., 2005, vol. 94, p. 205501.
24. K.F. Yao, F. Ruan, Y.Q. Yang, and N. Chen: *Appl. Phys. Lett*., 2006, vol. 88, p. 122106.
25. Y.H. Liu, G. Wang, R.J. Wang, D.Q. Zhau, M.X. Pan, and W.H. Wang: *Science*, 2007, vol. 315, pp. 1385–88.
26. J.J. Lewandowski, W.H. Wang, and A.L. Greer: *Philos. Mag. Lett*., 2005, vol. 54, pp. 77–87.
27. X.J. Gu, S.J. Poon, G.J. Shiflet, and J.J. Lewandowski: *Acta Mater*., 2010, vol. 58, pp. 1708–20.
28. X.J. Gu, S.J. Poon, G.J. Shiflet, and J.J. Lewandowski: *Scripta Mater*., 2009, vol. 60, pp. 1027–30.
29. J.M. Park, J. Jayaraj, D.H. Kim, N. Mattern, G. Wang, and J. Eckert: *Intermetallics*, 2010, vol. 18, pp. 1908–11.
30. X.F. Pan, H. Zhang, Z.F. Zhang, M. Stoica, G. He, and J. Eckert: *J. Mater. Res*., 2005, vol. 20, pp. 2632–38.
31. G. Wang, K.C. Chan, L. Xia, P. Yu, J. Shen, and W.H. Wang: *Acta Mater*., 2009, vol. 57, pp. 6146–55.
32. F.F. Csikor, C. Motz, D. Weygand, M. Zaiser, and S. Zapperi: *Science*, 2007, vol. 318, pp. 251–54.
33. A.S. Argon: *Acta Metall*., 1979, vol. 27, pp. 47–58.
34. M. Kusy, U. Kühn, A. Concustell, A. Gebert, J. Das, J. Eckert, L. Schultz, and M.D. Baro: *Intermetallics*, 2006, vol. 14, pp. 982–88.
35. J.M. Park, D.H. Kim, K.B. Kim, E. Fleury, M.H. Lee, W.T. Kim, and J. Eckert: *J. Mater. Res*., 2008, vol. 23, pp. 2984–89.
36. L.Q. Xing, Y. Li, K.T. Ramesh, J. Li, and T.C. Hufnagel: *Phys. Rev. B*, 2001, vol. 64, p. 180201.
37. Y.C. Kim, J.H. Na, J.M. Park, D.H. Kim, J.K. Lee, and W.T. Kim: *Appl. Phys. Lett*., 2003, vol. 83, pp. 3093–95.
38. D.C. Hofmann, J.Y. Suh, A. Wiest, G. Duan, M.L. Lind, M.D. Demetriou, and W.L. Johnson: *Nature*, 2008, vol. 451, pp. 1085–90.
39. U. Kühn, J. Eckert, N. Mattern, and L. Schultz: *Appl. Phys. Lett*., 2002, vol. 80, pp. 2478–80.
40. J.M. Park, J.H. Na, D.H. Kim, K.B. Kim, N. Mattern, U. Kühn, and J. Eckert: *Philos. Mag*., 2010, vol. 90, pp. 2619–33.
41. T. Richeton, J. Weiss, and F. Louchet: *Nature Mater*., 2005, vol. 4, pp. 465–69.
42. D. Pan, A. Inoue, T. Sakurai, and M.W. Chen: *Proc. Natl. Acad. Sci. USA*, 2008, vol. 105, pp. 14769–14772.
43. W.L. Johnson and K. Samwer: *Phys. Rev. Lett*., 2005, vol. 95, p. 195501.
44. M.L. Falk and J.S. Langer: *Phys. Rev. E*, 1998, vol. 57, pp. 7192–205.
45. J.S. Langer: *Phys. Rev. E*, 2004, vol. 70, p. 041502.
46. A.S. Argon: *The Physics of Strength and Plasticity*, MIT, Cambridge, MA, 1969.
47. K.F. Kelton: *J. Non-Cryst. Solids*, 2004, vol. 334, pp. 253–58.